75th International Astronautical Congress (IAC), Milan, Italy, 14/18 October 2024.

IAC-24-C1.IP.20

Long-term evolution of orbits in cislunar space: characterisation and stability analysis

Mathilda Bolis [a,*], **Elisa Maria Alessi**[b], **Camilla Colombo** [a]

[a] *Department of Aerospace Science and Technology, Politecnico di Milano, Via La Masa 34, 20156, Milan, Italy. mathilda.bolis@polimi.it, camilla.colombo@polimi.it*
[b] *Istituto di Matematica Applicata e Tecnologie Informatiche "Enrico Magenes", Consiglio Nazionale delle Ricerche, Via Alfonso Corti 12, Milano, 20133, Italy em.alessi@mi.imati.cnr.it*
[*]Corresponding author: mathilda.bolis@polimi.it

Abstract

Space is one of the last frontiers of scientific exploration and, now more than ever, it is also a valuable economic and strategic resource. The exponential increase in academic and industry's focus on space, empowered by the usage of CubeSats, has inevitably increased the amount of in-orbit objects. As space projects become more and more ambitious, the development of Space Situational Awareness (SSA) becomes more and more important. In this context, space agencies and companies have expressed a clear interest in the cislunar orbit realm, defined as an area going from hyper-geostationary (GEO) all the way to the Moon. On the one hand, the Lunar Gateway and the Artemis projects will require continuous and safe access to the lunar surface. On the other hand, the whole cislunar environment is being considered for exploration and scientific missions. The increase in the number of spacecraft in cislunar space can generate problems that, at least so far, have not been addressed in this region. To understand why this statement is true, it is enough to observe how the debris issue affects the vicinity of Earth to date. It cannot be excluded that a similar problem may arise in the future for cislunar space too, with greater complications due to the more complex and chaotic dynamic. Consequently, the design of the end-of-life phase of these missions is of particular interest.

In this paper, the complex dynamics in the Earth-Moon (EM) system will be analysed, employing the Circular Restricted Three-Body Problem (CR3BP) as a fundamental model. Leveraging differential corrections and continuation methods, it is possible to define equilibrium points and families of periodic orbits, including, for example, Halo or Near Rectilinear Halo Orbits (NRHOs). Insights related to the stability of these families of periodic orbits will be provided, computing different types of stability indicators, based on the linear dynamical behaviour but not only. This work aims to characterise orbital families in cislunar space from a stability standpoint. This allows deriving stability maps that can be used to identify proper solutions for end-of-life disposal for the families of orbits considered.

Keywords: periodic orbits, stability, cislunar space, end-of-life

Nomenclature

x [ndL]	Position along x
y [ndL]	Position along y
z [ndL]	Position along z
$\dot{x}$ [ndL/ndT]	Velocity along x
$\dot{y}$ [ndL/ndT]	Velocity along y
$\dot{z}$ [ndL/ndT]	Velocity along z
μ [ndL^3/ndT^2]	Mass parameter of the system
m_M [kg]	Mass of the Moon
m_E [kg]	Mass of the Earth
t [ndT]	Time
$\boldsymbol{\phi}(t, t0)$	STM evaluated between t_0, initial time and t_f, final time
ndL [-]	Non-dimensional Length
ndT [-]	Non-dimensional Time

Acronym/Abbreviations

2D	Two-dimensional
3D	Three-dimensional
4D	Four-dimensional
CoM	Center of Mass
EM	Earth-Moon
EoL	End-of-Life
EoM	Equations of Motion
GEO	Geostationary
JC	Jacobi Constant
NPCM	Natural Parameter Continuation Method
NRHO	Near Rectilinear Halo Orbit
PAM	Pseudo Arc-length Method
s/c	Spacecraft
STM	State Transition Matrix

1. Introduction

Space is one of the last frontier of human exploration: great steps forward have been taken since the first man stepped on the Moon, but a vast area of space still remains unexplored. In the last few years, near-Earth space has become increasingly important for many services and applications essential for life on Earth, including telecommunications, meteorological monitoring, navigation and scientific research. At the same time, many companies and agencies have expressed a clear interest in cislunar space, defined as an area extending from hyper-GEO up to the Lagrangian points of the EM system [1], scheduling missions such as the Artemis programme [2] or the Lunar Gateway [3].

The exponential growth in the number of objects in orbit has concurrently created new challenges to deal with, such as the growing space debris problem [4]. As more operational satellites are launched, the number of uncontrolled and potentially hazardous objects in orbit also rises, increasing the risk of collisions that could endanger current and future missions. To date, the debris problem is limited to near-Earth space: in the coming years, it will be crucial to implement mitigation and control strategies to ensure sustainable and safe access to it. Given the interest shown by several institutions towards cislunar space, it is easy to imagine how the problem of space debris could also arise in this less explored area of space.

One of the largest differences between near-Earth space and the cislunar region lies within the dynamics characterising them. The dynamics in the EM system is highly non linear and chaotic, due to the comparable gravitational influence of both Earth and Moon. This is one of the reasons why dealing with the space debris problem in cislunar space, as around the Earth today, could turn out to be much more complex than expected.

Probably the most effective mitigation measure that could be implemented to avoid this problem from the beginning is a careful design of the End-of-Life (EoL) phase of satellite missions. Once the operational mission is complete, a spacecraft must be decommissioned in a way that ensures that it no longer poses a risk to other satellites or future missions.

Several strategies have been developed to carry out and design the disposal at EoL of satellites orbiting Libration Point Orbits (LPO). For what concerns the EM system, in [5], it is proposed to develop a dynamical cartography of cislunar space. Samples are generated along several orbits chosen as case studies and, after applying a manoeuvre to each of their states, a random perturbation is introduced into the system and several Monte-Carlo simulations are performed. The robustness of each solution to possible perturbations is then assessed. For the Sun-Earth system, in [6], the EoL design for GAIA, orbiting Sun-Earth L_2, is formulated as a multi-objective optimisation problem. This approach is proposed for disposal with impact on the Moon, with destructive re-entry to Earth, and with insertion into a heliocentric orbit. For the latter case, an energy approach is suggested. This strategy is also proposed in [7] and [8], for the design of the disposal of a satellite with insertion into a heliocentric orbit. In [9], transfers from orbits in Sun-Earth L_1 and L_2 to the Moon are analysed. The conditions under which the satellite impacts the Moon or is weakly captured by it are examined. In addition to Moon impact, Earth re-entry is also considered a possible EoL solution, although it is a complex and sometimes operationally risky option [10]. The option of atmospheric re-entry, compared to others, must be accompanied by a careful assessment of the associated risks [6]. Some strategies developed in these contexts could be applied to cislunar space.

This work aims to explore the dynamical structure of cislunar space, exploiting the CR3BP as a fundamental model, and looking for stable and chaotic behaviours. By leveraging Poincaré maps, stability index, and the maximum local Lyapunov exponent, the aim is to characterise the dynamics of this area of space from a stability standpoint. This would allow this inherent chaotic nature of the system to be exploited to seek low-cost disposal solutions that are favourable from a dynamic point of view.

The article is organised in three main sections. The first focuses on the dynamical model, outlining how its characteristics can be used to design periodic orbits. The second focuses on the description of the different types of stability indicators, analysing their trend along families of orbits. Finally, a case study is presented focusing on the disposal of possible satellites placed on some orbits belonging to the Halo family around L_2 in the EM system, offering a preliminary insight into the relationship between disposal cost and orbital stability.

2. Circular Restricted Three Body Problem

The CR3BP [11] is a dynamical model that reasonably approximates the complex dynamics characterising the cislunar space. It describes the motion of a massless object under the gravitational influence of two major bodies, the Earth and the Moon in the case considered, rotating around their common Centre of Mass (CoM) in circular orbits. The Equations of Motion (EoMs) are expressed in synodic coordinates. The x-axis is defined as the line connecting the two major bodies, with the origin being the CoM of the system. The y-axis is perpendicular to the x-axis and lies within the EM plane, while the z-axis is perpendicular to it. All quantities are dimensionless. Lengths are scaled with respect to the EM distance, and times in such a way that the mean motion of the reference system is equal to 1. When indicating a quantity, ndL identifies the non-dimensional length, and ndT is the non-dimensional time. The EoMs char-

acterising the CR3BP are:

$$\ddot{x} = 2\dot{y} - \frac{\partial U}{\partial x}, \ddot{y} = -2\dot{x} - \frac{\partial U}{\partial y}, \ddot{z} = -\frac{\partial U}{\partial z} \quad (1)$$

where $U(x, y, z)$ is defined as:

$$U = -\frac{1}{2}(x^2 + y^2) - \frac{1-\mu}{r_1} - \frac{\mu}{r_2} - \frac{1}{2}\mu(1-\mu) \quad (2)$$

and:

$$r_1 = ((x+\mu)^2 + y^2 + z^2)^{1/2} \quad (3)$$

$$r_2 = ((x-1+\mu)^2 + y^2 + z^2)^{1/2} \quad (4)$$

where μ is the mass parameter of the system, defined as the ratio between the mass of the Moon, m_M, and the sum of the masses of the Earth and the Moon, $m_E + m_M$:

$$\mu = \frac{m_M}{m_E + m_M} \quad (5)$$

where, for the EM system, μ is equal to 0.0121506 ndL^3/ndT^2. A schematic representation of the model can be found in Figure 1.

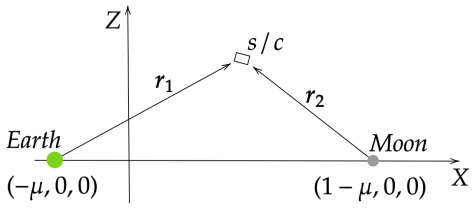

Fig. 1. CR3BP - Schematic representation.

The CR3BP is an Hamiltonian system, independent on time and with three degrees of freedom. It is possible to define only one integral of the motion, commonly identified as the Jacobi Constant (JC), or Jacobi Integral:

$$JC = -(\dot{x}^2 + \dot{y}^2 + \dot{z}^2) - 2U \quad (6)$$

In the framework of the CR3BP, there exist five equilibrium points belonging to the plane of the two major bodies, known as Lagrange or Libration points. Among these, L_2, L_1, and L_3 lie along the x-axis of the synodic reference frame and are referred to as collinear Lagrange points. The remaining two points, L_4 and L_5, are termed triangular Lagrange points and form the vertices of equilateral triangles defined by the two larger bodies.

3. Periodic orbits

Periodic orbits are trajectories that repeat after a certain amount of time, called a period, in the synodic reference frame. In a three-body system, several types of periodic orbits can be defined. Generally, these orbits evolve around one of the five Lagrange points or one of the two major bodies. The CR3BP is particularly suited for the definition of periodic orbits in the EM system because the classical formulation used to design them is based on some of its symmetry properties. In Section 3.1 and Section 3.2, the numerical techniques used to compute periodic orbits are defined, and in Section 3.3 some results are presented. It is important to note that not all families of periodic orbits are considered in this analysis. Some may be identified by making slight adjustments to the method described herein, while others necessitate the definition of different methodologies.

3.1 Numerical computation of periodic orbits

A family of periodic orbits is generated thanks to a differential correction algorithm [12]. A generic state of the system can be defined as $\boldsymbol{x} = [x\ y\ z\ \dot{x}\ \dot{y}\ \dot{z}]^T$. Periodic orbits of interest for the analysis presented herein are symmetric about the xz-plane, and intersect this plane perpendicularly. Thus, the state at which the trajectory will intersect the xz-plane at time t_0 can be defined as:

$$\boldsymbol{x_0}(t_0) = [x_0\ 0\ z_0\ 0\ \dot{y}_0\ 0] \quad (7)$$

A periodic orbit will intersect the xz-plane orthogonally once more after half a period, at a time t_f. So, the desired state at time t_f will be:

$$\boldsymbol{x_f}^d(t_f) = [x_f\ 0\ z_f\ 0\ \dot{y}_f\ 0] \quad (8)$$

For dynamical models such as the CR3BP, the linear relationship between variations on the initial and on the final state can be expressed as:

$$\delta\boldsymbol{x}(t) = \boldsymbol{\phi}(t, t_0)\delta\boldsymbol{x}(t_0) \quad (9)$$

where $\boldsymbol{\phi}(t, t_0)$ is the State Transition Matrix (STM) of the CR3BP dynamics. Equation 9 can be used to trace the displacement that must be imposed on the initial state to obtain a desired final state. Propagating the initial state $\boldsymbol{x_0}(t_0)$ between 0 and t_f, the final state $\boldsymbol{x}_f(t_f)$ is obtained. Since three of the components of the final desired state are known and $\delta\boldsymbol{x}(t_f) = \boldsymbol{x_f}^d(t_f) - \boldsymbol{x}_f(t_f)$, it is possible to compute the unknown components of $\delta\boldsymbol{x}(t_0)$ by inverting Equation 9. A new, modified, initial state is found, equal to $\hat{\boldsymbol{x}}_0 = \boldsymbol{x}_0 + \delta\boldsymbol{x}_0$. The process is iterated until the value of $\delta\boldsymbol{x}(t_f)$ does not become smaller than a fixed tolerance.

All the unknowns, including the final time t_f, can be computed by slightly modifying the process described above. The vector of the unknowns is:

$$\boldsymbol{a}(t_0) = [x_0 \ z_0 \ \dot{y}_0 \ t_f]^T \tag{10}$$

Instead, $\boldsymbol{b}(t_f) = [y_f \ \dot{x}_f \ \dot{z}_f]$ is defined, such that $\delta\boldsymbol{b}(t_f) = \boldsymbol{b}_f{}^d(t_f) - \boldsymbol{b}_f(t_f)$ can be identified. Since:

$$\delta\boldsymbol{b}(t_f) = \boldsymbol{A} \ \delta\boldsymbol{a}(t_0) \tag{11}$$

The matrix $\boldsymbol{A}$ is defined such as:

$$\boldsymbol{A} = \begin{bmatrix} \phi_{yx} & \phi_{yz} & \phi_{y\dot{y}} & \dot{y}(t_f) \\ \phi_{\dot{x}x} & \phi_{\dot{x}z} & \phi_{\dot{x}\dot{y}} & \ddot{x}(t_f) \\ \phi_{\dot{z}x} & \phi_{\dot{z}z} & \phi_{\dot{z}\dot{y}} & \ddot{z}(t_f) \end{bmatrix} \tag{12}$$

where ϕ_{ij} is the component of the STM evaluated between t_0 and t_f and relative to the variables i and j. The solution to the problem is found with a Newton-like algorithm, iterating the process mentioned above.

Since there is one more unknown than the number of equations, the problem is underdetermined. Its resolution can lead to multiple, possibly incorrect solutions. For this reason, to obtain a correct solution and avoid inaccuracies, it is necessary to choose initial guesses close to the exact solution.

3.2 Continuation methods

As stated in the above Section, the numerical computation of periodic orbits requires good initial guesses, close to the correct solution. For each family of periodic orbits computed, a first initial guess, used for a single first orbit, is known. Then, continuation methods are employed to determine initial guesses for other orbits belonging to the family. Three types of continuation algorithms are used: the Natural Parameter Continuation Method (NPCM) of order one [13], along x and z, and the Pseudo Arc-length Method (PAM) [14].

When employing the NPCM, a continuation variable denoted by γ, which can be chosen, for example, as x_0 or z_0, must be selected: x_0 is the component of the solution to the differential correction algorithm relative to the position along x, z_0 to that along z. Given the solution leading to the definition of orbit number 1, $\boldsymbol{a}_1(t_0)$, an initial guess for the computation of the unknowns of orbit number 2, $\hat{\boldsymbol{a}}_2(t_0)$, must be found. Regarding the continuation variable, its value as an initial guess for orbit 2 can be computed as follows:

$$\hat{\gamma}_2 = \gamma_1 + \varepsilon \tag{13}$$

where ε is chosen in a range between 10^{-4} and 10^{-5}. The initial guesses for the elements of $\hat{\boldsymbol{a}}_2(t_0)$ other than the continuation variable, collected in the vector $\hat{\boldsymbol{z}}_2$, are defined through the equation:

$$\hat{\boldsymbol{z}}_2 = \boldsymbol{z}_1 + \varepsilon\dot{\boldsymbol{z}}_1 \tag{14}$$

where $\dot{\boldsymbol{z}}_1 = \boldsymbol{C}\backslash\boldsymbol{d}$, and:

- $\boldsymbol{C}$ is the Jacobian of the solution $\boldsymbol{a}_1(t_0)$, from which the column related to the continuation variable is eliminated
- $\boldsymbol{d}$ is instead equal to this column

The PAM involves instead parameterising the continuation function with respect to its arclength. This method is more robust in the presence of critical points and bifurcations compared to the previous one. In this approach, the cost function of a zero-finding algorithm is modified by adding a final equation that imposes the solution at the $(i+1)$-th step to be perpendicular to the tangent to the continuation function at the i-th step.

3.3 Families of periodic orbits

Several families of periodic orbits have been computed using the techniques described in the previous Sections. In cislunar space, when considering the CR3BP, numerous families of periodic orbits bifurcating from Libration points can be defined [15]. Herein, a limited selection of these families is presented, and will be used as a case study for the following stability analysis. It is important to note that from a purely mathematical standpoint, it is possible to define a family of periodic orbits even with a perigee radius smaller than that of the Moon. However, since related to more practical applications, the results presented are limited to orbits with a perigee radius greater than or equal to that of the Moon.

Halos are perhaps the most well-known among the periodic orbits belonging to families defined in cislunar space. Two Halo families are presented, one bifurcating from EM-L_1, shown in Figure 2b, and the other from EM-L_2, shown in Figure 2a. The orbits are represented as function of their perilune radius, defined as their minimum distance from the Moon. Each Halo family divides into two branches, a southern and a northern one, but it is chosen to show only the southern branch. The two branches are symmetrical with respect to the z-axis of the synodic reference frame. Of particular interest are Halo orbits belonging to the family originating from EM-L_2 that are situated closely to the Moon. These orbits are known as Near Rectilinear Halo Orbits (NRHO) and exhibit specific stability characteristics, making them of interest for numerous applications.

Several families of planar periodic orbits are also computed, selected from those defined in [16]. Two of these families bifurcate from EM-L_1 and EM-L_2: they are the 2D equivalent of Halo orbits. These orbits are identified both as Lyapunov and as family-*c*, when bifurcating from L_1, and family-*a*, when bifurcating from L_2 [16]. These two families are shown in Figure 2d and Figure 2c.

Finally, two families of quasi-satellite orbits rotating around the Moon are computed. These families consist of retrograde, highly stable orbits associated with high energy levels, identified as family-*f* and family-*g*. They are illustrated respectively in Figure 2e and Figure 2f.

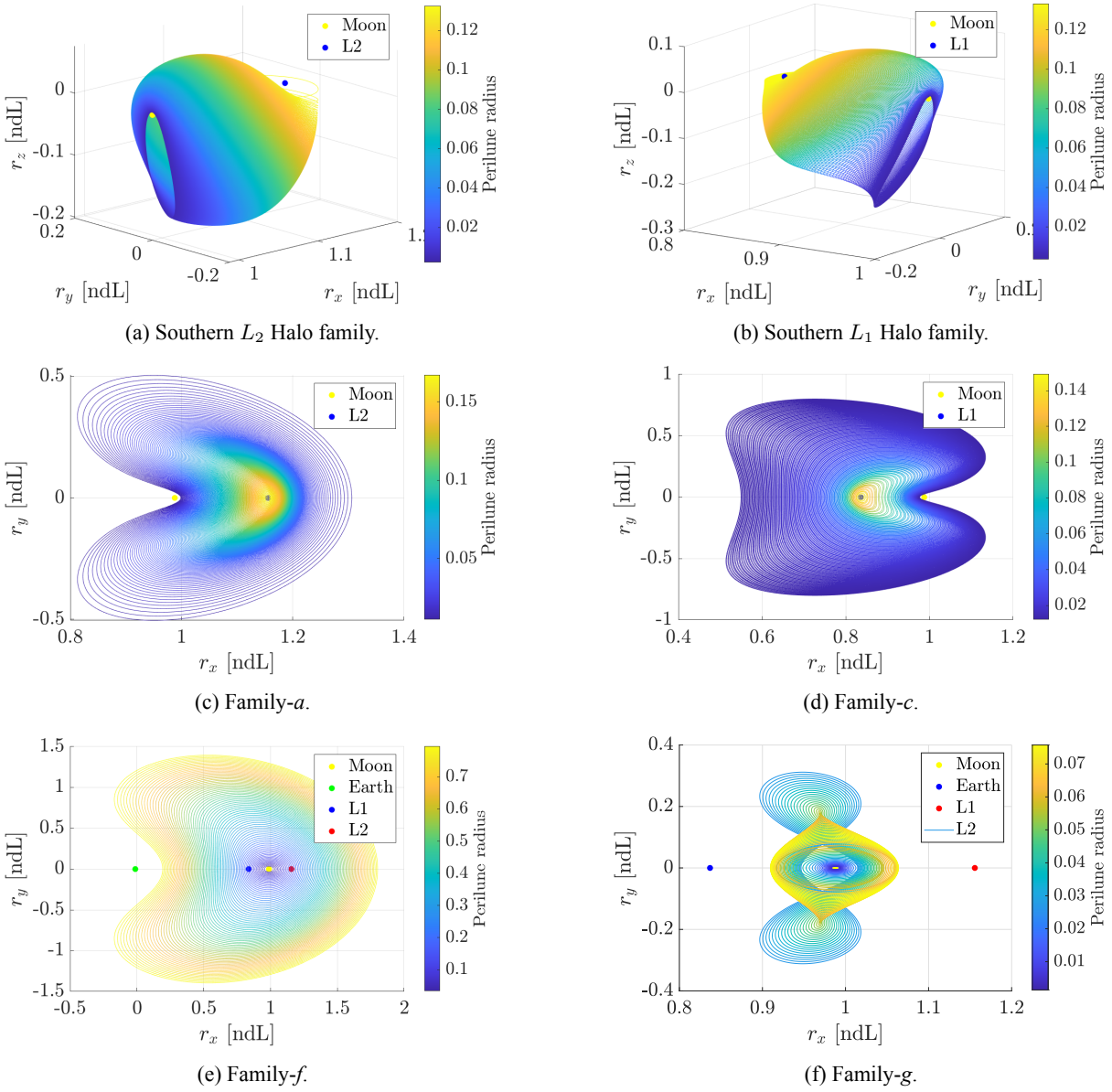

(a) Southern L_2 Halo family.

(b) Southern L_1 Halo family.

(c) Family-*a*.

(d) Family-*c*.

(e) Family-*f*.

(f) Family-*g*.

Fig. 2. Families of periodic orbits considered in the analysis.

4. Stability and chaoticity

Assessing the stability and the chaoticity of families of periodic orbits in cislunar space is of interest for many practical applications. For example, it is assumed that satellites orbiting along highly stable trajectories will incur low station-keeping and, vice-versa, high disposal costs. Stability refers to the orbit's ability to remain unaffected by minor perturbations [17], chaoticity is instead related to the stochastic behaviour of a deterministic physical system, resulting in the tendency of two infinitely close initial conditions to generate two very different final results [18]. These two concepts, even if related, must be investigated separately. Various techniques, described in the following Sections, are applied to analyse the stability and the chaoticity of trajectories in cislunar space.

4.1 Linear stability and stability index

The linear stability or instability of a periodic orbit can be determined by analysing the eigencouples, eigenvalues and eigenvectors, of its monodromy matrix, $\boldsymbol{M}$, defined as the STM computed after one orbital period, $\boldsymbol{\phi}(t_0, T)$ [19]. To reduce the possibility of encountering numerical errors, $\boldsymbol{\phi}(t_0, T)$ is not obtained directly through integration between t_0 and T but is derived from the STM evaluated at half a period, $\boldsymbol{\phi}(t_0, T/2)$. This approach is made feasible by a set of mathematical transformations that exploit the symmetry of the problem with respect to the x-axis of the synodic reference frame [19]. Also, note that $\boldsymbol{\phi}(t_0, T/2)$ is retrieved directly from the differential correction algorithm used to design periodic orbits: since it is derived from a condition fixed to guarantee periodicity, its evaluation is less af-

fected by numerical errors than that of $\phi(t_0, T)$.

Once $\boldsymbol{M}$ is evaluated, its eigenvalues are computed. If λ is a real eigenvalue of the system, $1/\lambda$ is also an eigenvalue of the system. Moreover, if λ^* is a complex eigenvalue of the system, its complex conjugate $\bar{\lambda}^*$ is also an eigenvalue of the system [20]. For a generic periodic orbit computed in the CR3BP, six eigenvalues exist. If, on the other hand, the orbit is planar, the eigenvalues are four. Since the orbit being analysed is periodic, a pair of eigenvalues always equals one [19]. For the remaining pairs, it is possible to identify:

- Stability: complex conjugate eigenvalues belonging to the unit circle indicate a stable behaviour
- Instability: real eigenvalues not belonging to the unit circle indicate an unstable behaviour
- Complex instability: complex eigenvalues not belonging to the unit circle indicate the presence of bifurcations, concept that exemplifies that of complex instability [21]

Since one pair of eigenvalues is trivial, in the 3D case it could be easier and more accurate to compute only the 2 non trivial couples of eigenvalues. A reduced monodromy matrix is defined as:

$$\begin{bmatrix} \delta x_T \\ \delta z_T \\ \delta \dot{x}_T \\ \delta \dot{z}_T \end{bmatrix} = \boldsymbol{M_{red}} \begin{bmatrix} \delta x_0 \\ \delta z_0 \\ \delta \dot{x}_0 \\ \delta \dot{z}_0 \end{bmatrix} \tag{15}$$

since $\delta y_0 = \delta \dot{y}_0 = 0$. The procedure used to obtain $\boldsymbol{M_{red}}$ from $\boldsymbol{M}$ is defined in [19]. The same procedure can be applied to the 2D case: having also $\delta z_0 = \delta \dot{z}_0 = 0$, only one couple of non-trivial eigenvalues will be computed.

Finally, the evaluation of the stability of a periodic orbit can be carried out through the calculation of a stability index, defined as [19][22]:

$$SI = \frac{1}{2} \left| \left(\lambda_{max} + \frac{1}{\lambda_{max}} \right) \right| \tag{16}$$

where λ_{max} is the maximum eigenvalue of $\boldsymbol{M_{red}}$. For $SI < 1$ the periodic orbit is considered stable. If a simple-periodic orbit has $SI = +1$, it is called a critical orbit of first or second type [22].

In the literature, different approaches to defining the stability index exist. The aforementioned formulation is equivalent to state that stability is guaranteed when the trace of the monodromy matrix ranges within ± 4 [23], since, as stated in [24]:

$$tr(\boldsymbol{M}) \simeq 1 + 1 + \lambda_{max} + \frac{1}{\lambda_{max}} \tag{17}$$

The trace of the monodromy matrix can be approximated as such since, also for the 3D case in which the eigenvalues are 6 in total, two of them are always complex conjugate with a small real part.

4.2 Poincaré maps

Poincaré maps are valuable tools for performing trajectory design in complex dynamical systems [13]. They can also be exploited to numerically evaluate the stability of a trajectory in the phase space, given a certain energy level.

In the context of the planar CR3BP, the definition of the complete state of a particle requires knowledge of its position (x,y) and velocity $(\dot{x}, \dot{y})$. This corresponds to a point in a four-dimensional phase space [25]. Consider searching for all the intersections of a trajectory with a proper surface of section, let it be $y = 0$. The crossings are searched when in the positive direction, with a fixed sign of $\dot{y}$, so for $\dot{y} > 0$.

Having fixed y, three more variables (x, $\dot{x}$, $\dot{y} > 0$) must be defined to characterise a point completely. As stated in previous Sections, within the CR3BP one integral of the motion, JC, can be defined. For a fixed value of JC, one component less of the complete state is needed to characterise a point. So, having fixed JC, $\dot{y} > 0$ can be found as a function of it and the other two non-zero state variables (x, $\dot{x}$). The phase space defined by these two variables and representing the returns of a trajectory on the previously chosen surface of section is called a Poincaré map.

After obtaining a Poincaré map for a specific area of the phase space, it is possible to identify periodic and quasi-periodic behaviours thanks to it. The crossings of a periodic trajectory with the surface of section always occur at the same point of the phase space. On the other hand, trajectories that do not exhibit periodic or quasi-periodic behaviours have irregular returns to the map. Figure 3 shows schematically the returns generated by two different types of trajectories:

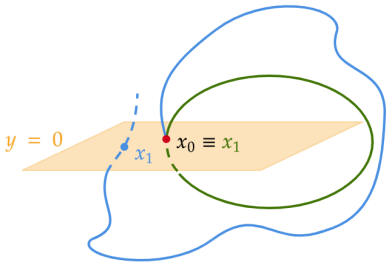

Fig. 3. Poincaré map - Schematic representation. In green, the behaviour of the first return of a periodic trajectory. In blue, the behaviour of the first return of a generic non-periodic trajectory.

Poincaré maps can also be obtained when considering the 3D spatial CR3BP. However, the results obtained may become quite challenging to interpret. A Poincaré map provides a way to reduce the phase space of a system by two variables. In a 3D scenario, this implies that four variables would still need to be mapped

to fully characterise the system. Representing a 4D map could be a challenging task, that can be addressed, for example, by using colours to represent the fourth dimension. But, when representing the returns of a 3D trajectory in a 4D phase space, a periodic or quasi-periodic trajectory will not be easily identified anymore by the same repeating patterns described for the planar case [26]. For these reasons, the analysis presented herein is limited to the planar CR3BP.

4.3 Maximum local Lyapunov exponent

Lyapunov exponents are a classical tool used to estimate the rate of divergence between two initially infinitely close solutions. They are indexes measuring the chaoticity of a trajectory. As many exponents can be analysed as the dimensions of the system but, typically, only the maximum Lyapunov exponent is computed. This value indeed provides the maximum excursion associated with two neighbouring orbits [27]. The more the value of the maximum Lyapunov exponent, L_λ, is large and positive, the more even a small perturbation will be greatly amplified [28]. For continuous dynamical systems, L_λ can be computed as:

$$L_\lambda = \lim_{t\to\infty} \frac{1}{t} \ln \left(\frac{||\delta \boldsymbol{x}(t)||}{||\delta \boldsymbol{x_0}(t_0)||} \right) \tag{18}$$

where $\delta \boldsymbol{x_0}(t_0)$ is an infinitesimal perturbation whose growth is to be estimated. For a periodic orbit, also knowing the relationship defined in Equation 9, the value of L_λ can be expressed as:

$$L_\lambda = \frac{1}{t^*} \ln \sqrt{\lambda_{max}} \tag{19}$$

where λ_{max} is the maximum eigenvalue related to the matrix $\boldsymbol{\phi}(t_0, t^*)\boldsymbol{\phi}^T(t_0, t^*)$, and $\boldsymbol{\phi}(t_0, t^*)$ is the STM of the system evaluated at $t = t^*$. The time t^* can be arbitrarily chosen and is, in this case, fixed equal to 1 day [28]. Instead, the time t_0 is associated with a generic initial state belonging to a periodic orbit. Accordingly, the formulation of Lyapunov's maximum exponent is 'local' and varies with respect to the initial state considered for the analysis.

4.4 Cislunar space: a stability analysis

In this Section, an analysis of the tendency towards instability and chaoticity that characterises cislunar space is presented. First, Poincaré maps covering a large area of cislunar space are generated. This will allow to identify periodic and quasi-periodic behaviours. Then, using the tools outlined in the previous Sections, the stability and the chaoticity of the families of periodic orbits presented in Section 3.3 are analysed.

Poincaré maps can be used to visualise regions of periodic and quasi-periodic behaviour in cislunar space. In Figure 4, Poincaré maps covering a substantial region of this area are presented, each corresponding to a different energy level.

The maps are obtained by defining a grid of initial conditions, with x ranging from -0.4 to 1.2 and $\dot{x}$ ranging from -2.5 to 2.5. For each selected value of JC, all the grid points are examined, to identify which correspond to states of potential orbiting objects. The value of $\dot{y}$ is calculated as a function of JC, x, and $\dot{x}$, and any points where $\dot{y}$ is complex are discarded. The remaining initial conditions are then propagated over one year, with all returns to the selected surface of section ($y = 0$) in the positive direction ($\dot{y} > 0$) being sampled and plotted in the phase space.

Each initial grid point is assigned a specific colour, which remains consistent for all mapped returns associated with its propagation. This approach allows for the identification of which states from the grid lead to chaotic structures and which result in regular, periodic, or quasi-periodic patterns. It is possible to distinguish regions of the phase space where objects are drawn toward stable periodic or quasi-periodic orbits, and regions where objects exhibit more chaotic behaviour.

Equilibrium points can be identified on the maps, representing initial conditions for designing periodic orbits. Specific geometries, such as circles and ellipses, correspond to quasi-periodic orbits.

Note that Figure 4 does not show the complete map of returns, but only a region of interest, with which cislunar space can be identified. Outside the observed zone, no periodic or quasi-periodic behaviour is observed, but chaos dominates. Indeed, the EM CR3BP approximates reality within a limited area of space, which can be identified as cislunar space. Beyond this, the behaviour of the visualised trajectories becomes less and less realistic and, more importantly, increasingly chaotic: as the distance from the major attractive bodies is increased, the velocity of the trajectories gradually increases, as moving away from the system. This is important to emphasise because some of the returns obtained by propagating the grid of initial conditions are not shown by Figure 4, and the overall structure of the phase space is much more chaotic than it appears.

Looking at the maps, some interesting behaviours can be observed. To the left of the Earth, only one family of periodic orbits is identified. These are circular retrograde quasi-satellite orbits. As the energy increases, this family of orbits gradually tightens, drawing closer to the Earth. To the right of the Earth, looking at the central section of the map, multiple families of periodic orbits can be observed instead, with their appearance varying significantly depending on the energy level considered. Notably, the number of identifiable families increases as the system's energy rises, with additional families of orbits gradually forming to the left of the Moon. For very high energy values, periodic and quasi-periodic structures become more evident. The number of returns visualised in the mapped section of cislunar space increases, and overall, the system appears less

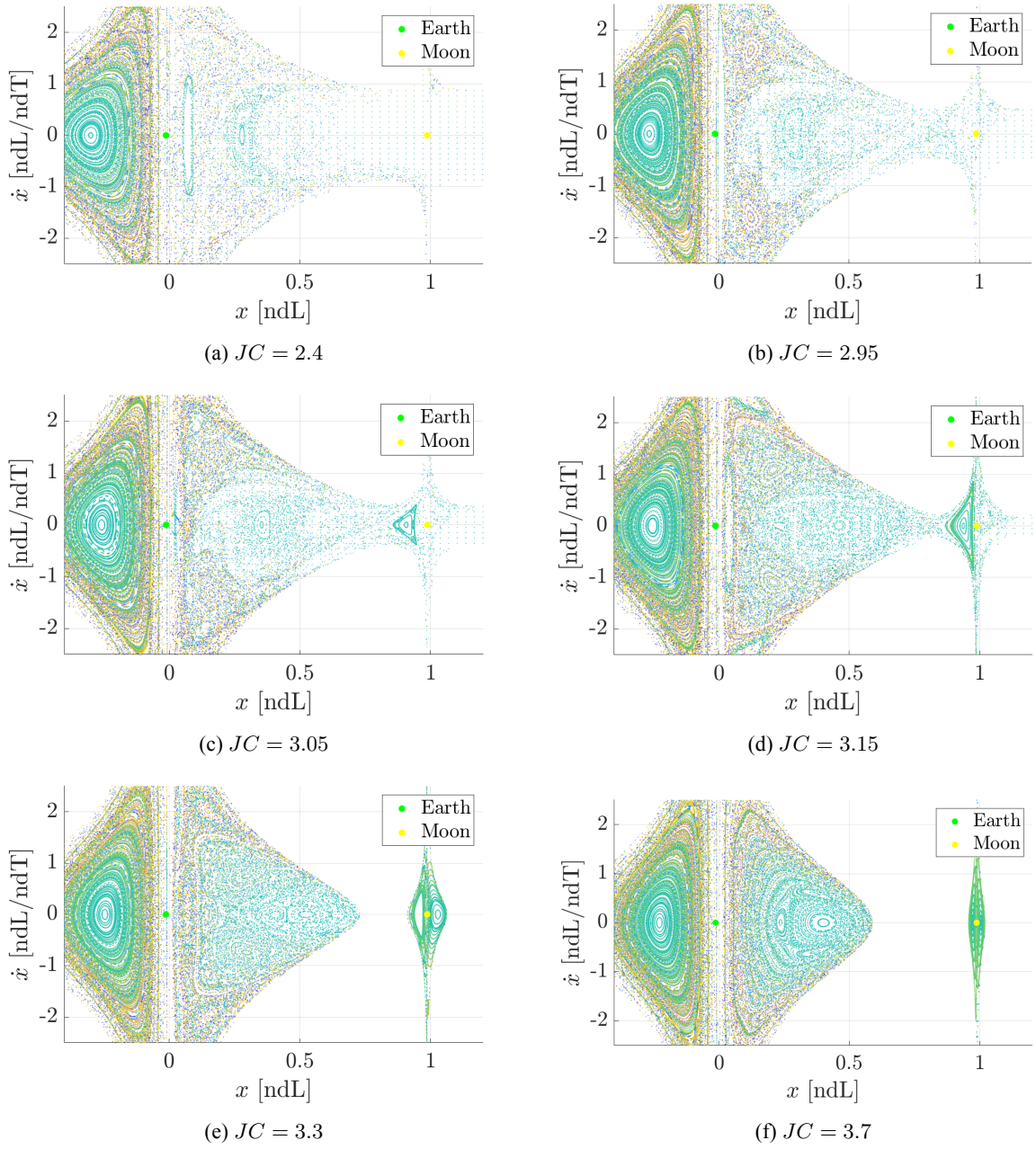

(a) $JC = 2.4$ (b) $JC = 2.95$

(c) $JC = 3.05$ (d) $JC = 3.15$

(e) $JC = 3.3$ (f) $JC = 3.7$

Fig. 4. Poincaré maps of cislunar space for different values of Jacobi Constant.

chaotic. As the energy level rises, the link connecting the Earth and the Moon closes, as the one between L_2, to the right of the Moon, and the outer solar system. This represents the closing of zero velocity curves, which occurs at L_1 and L_2 for JCs above their respective thresholds. To open or close these links, the energy level of the system must be adjusted, as indicated by the maps. This means that it becomes increasingly challenging to perform transfers from around the Moon to Earth's vicinity as the energy level rises, leading to the closure observed in the maps.

Thanks to Poincaré maps, some general considerations are made regarding stable and chaotic behaviours in cislunar space. The stability and the chaoticity of the families of periodic orbits mentioned in Section 3.3 are examined instead thanks to the stability index and the maximum local Lyapunov exponent. In Figure 5, the relationship between the stability index, the JC, and the perilune radius for the different orbit families is shown.

In Figure 5a, this trend is reported for Halo families in L_1 and L_2, family-*a* and family *c* [16]. It can be observed that for all four families of orbits bifurcating from L_1 and L_2, both the stability index and the JC are low when the orbits are in the vicinity of the Moon. These orbits, therefore, correspond to both high stability and low energy levels. In the case of the Halo families near EM-L_2 and L_1, these orbits are identified as

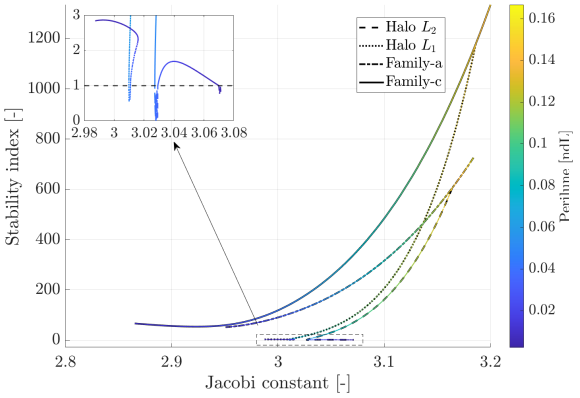

(a) Stability analysis: Halo in EM-L_2 and EM-L_1, family-*a* and family-*c*.

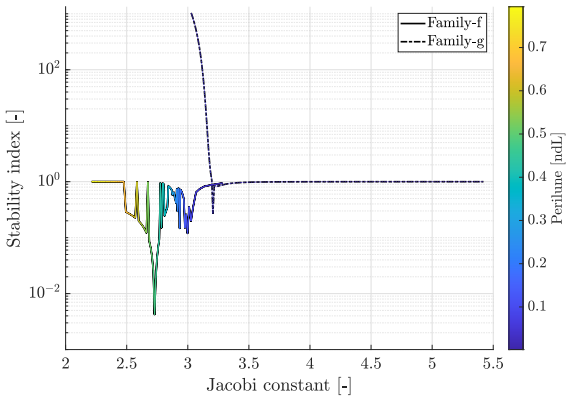

(b) Stability analysis: family-*f* and family-*g*.

Fig. 5. Relationship between stability index, Jacobi constant and perilune radius for several families of periodic orbits in cislunar space.

NRHOs. The only stable orbits (i.e., those with $SI < 1$) within these families are located between the Halo families in both EM-L_2 and L_1, at energy levels around 3.01, 3.03, and 3.07, as shown in the zoomed-in section of Figure 5a. In contrast, orbits farther away from the Moon, particularly near L_1 and L_2, are associated with high energy levels and high instability.

In Figure 5b, the relationship between the stability index, JC, and the perilune radius is shown instead for orbits belonging to family-*f* and family-*g* [16]. Orbits from family-*f* are retrograde, planar, and exhibit high stability, especially if close to the Moon. Some periodic orbits from this family can be observed to the immediate left of the Moon in Figure 4c and Figure 4d. In contrast, orbits from family-*g* are also retrograde and planar, but they are not as stable as those in family-*f* and have very low perilunes for the entire family. When stable, they can be seen in the maps of Figure 4, to the right of the Moon. These orbits appear in the map only at higher values of JC. Indeed, in Figure 5b, they are shown to be stable for high values of JC, around 3.3, and, as the energy increases, they become quasi-stable.

Finally, the trend of the maximum local Lyapunov exponent is computed for all orbit families. It is important to note that, unlike the stability index, L_λ provides a local measure of chaoticity. For the stability index, a single value was associated with an entire orbit, whereas in this case, a value of L_λ is assigned to each point of a single orbit. Furthermore, it is important to remember that L_λ is related to chaoticity rather than stability. In Figure 6, the behaviour of the maximum local Lyapunov exponents for the different families of periodic orbits is shown as a function of both the phase angle and the JC. The phase angle is defined as the angle swept by an ideal satellite travelling along the periodic orbit over a given amount of time, and it is computed as:

$$\vartheta = 2\pi \frac{\hat{t}}{T} \tag{20}$$

where $\hat{t}$ is the time elapsed since the satellite began moving along the orbit, and T is the orbital period. For the 3D families of orbits, $\vartheta = 0$ correspond to the intersection of the orbit with the xz-plane when $z < 0$. For the 2D ones $\vartheta = 0$ corresponds to the intersection of the orbit with the x-axis when $\dot{y} > 0$. This happens for families *a* and *c* to the right of respectively L_2 and L_1, and for families *f* and *g* to the left of the Moon.

The significant variations in the value of L_λ that are observed along a single orbit can be attributed to the fact that the maximum Lyapunov exponent is a local indicator of chaos rather than a global one. For prograde orbits, L_λ shows peaks that correlate with both a decreasing JC and a decreasing distance to the Moon. For Halo orbits in L_1 and L_2, L_λ decreases with decreasing JCs at phase angles near $0°$ and $360°$. At the same time, for low JCs, peaks emerge at phase angles approximately equal to $120°$ and $180°$. This is probably due to the Moon's gravitational influence on the orbits when these phase angles are swept, a condition whereby the distance to the Moon is minimised, resulting in more chaotic behaviour. A similar trend is observed in family-*c*, where only one peak occurs at low JCs for phase angles about $180°$, where the distance to the Moon is minimal. In family-*a*, peaks are observed around $0°$ and $360°$, again coinciding with low JCs and the minimum orbit-Moon distance. This indicates that family-*a* follows a similar pattern to the other orbit families bifurcating from L_1 and L_2.

The trends for family-*f* and family-*g* differ slightly; L_λ remains high, but constant, for high JCs, which corresponds to the minimum distance between the orbits and the Moon. For family-*f*, two peaks can be identified at low JCs and phase angles near$0°$ and $360°$. This

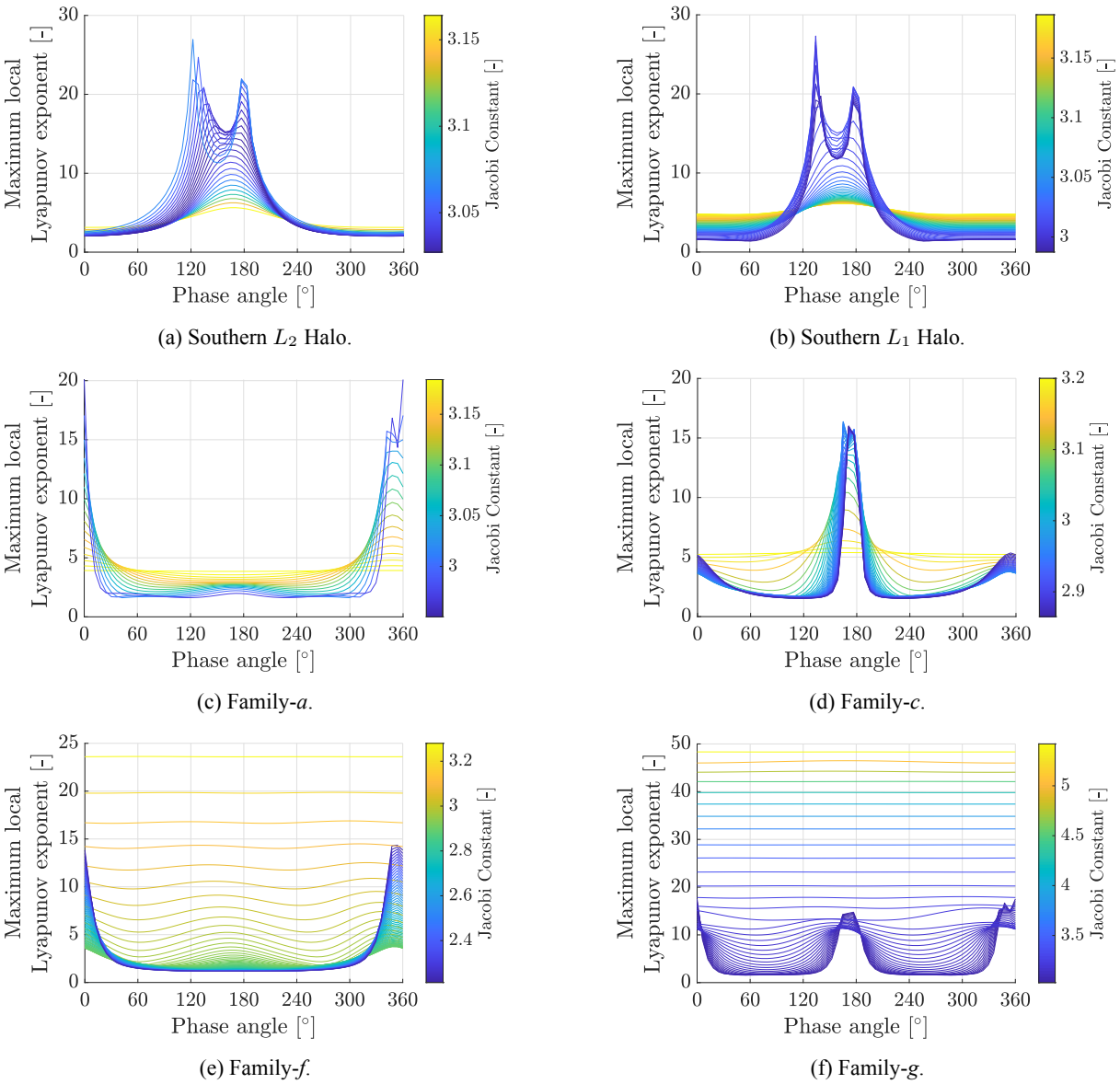

(a) Southern L_2 Halo.

(b) Southern L_1 Halo.

(c) Family-*a*.

(d) Family-*c*.

(e) Family-*f*.

(f) Family-*g*.

Fig. 6. Maximum local Lyapunov exponents for different families of periodic orbits, as function of phase angle and Jacobi Constant.

corresponds to a condition where the maximum local Lyapunov exponent is calculated for points that lie exactly between the Earth and the Moon. The combined gravitational influences of the two bodies increase the chaotic tendency of the system.

5. Disposal at end-of-life

When referring to EoL disposal, the final phase of a satellite mission is addressed, which occurs once its primary scientific objectives have been achieved.

This phase aims to ensure the satellite is disposed of safely, minimising the risk it poses to current and future missions. Two main requirements guide the design of the EoL phase: firstly, the satellite must not become a hazard for other missions, and secondly, disposal strategies must be cost-effective.

Studies on EoL disposal in the cislunar environment focus on one of the following four strategies:

- Insertion into a heliocentric trajectory
- Impact on the Moon
- Earth re-entry
- Insertion into a stable cislunar graveyard orbit

An analysis of the stability behaviour and chaotic dynamics of cislunar space can help define particularly cost-effective disposal strategies.

As discussed in previous Sections, cislunar space is characterised by highly unstable and chaotic dynamics, and regions of both chaotic and periodic or quasi-periodic behaviour can be identified. While the chaotic nature of the dynamics makes trajectory design complicated, there is an opportunity to exploit it to search

for low-cost EoL disposal solutions. For example, it is possible to assume that highly unstable or chaotic periodic orbits could provide cost-efficient EoL solutions. Instead, Poincaré maps can be used as a valuable tool to identify initial conditions for designing stable periodic or quasi-periodic orbits. These orbits can serve as potential graveyards, possible destinations for safe disposals.

In the following Section a case study is outlined, to illustrate the validity of some of these hypothesis.

5.1 Heliocentric disposal: case study

In this Section, heliocentric disposal is designed for some orbits of the Halo family in EM-L_2. This family of orbits was chosen because it is the one on which the application of this disposal method is most straightforward. The goal is to analyse how high instability can lead to cost-effective disposal. An energetic approach is used for the manoeuvre design [6] [7] [8].

In this work, when referring to heliocentric disposal, the spacecraft will be inserted in an exiting L_2 graveyard. This means that an EoL trajectory is designed such that, once it exists L_2, the zero velocity curves of the EM CR3BP are closed so that the satellite can not return to cislunar space. This, however, does not guarantee that the trajectory is a heliocentric one. To verify whether the satellite is correctly disposed outside the solar system, it would be necessary to introduce the effect of the Sun into the model as well, designing a trajectory that also exits Sun-Earth L_2 and then closing the Sun-Earth zero velocity curves as well. The development of such a model will be presented in future work. Meanwhile, it is believed that the definition of a safe area limited to cislunar space is still relevant to the objectives of this work.

The disposal is designed as a two-impulse manoeuvre: the first ΔV aims to move away from the periodic orbit in the most dynamically efficient way, and the second to close the zero velocity curves once beyond L_2, preventing the satellite from re-entering cislunar space.

Initially, the unstable manifold is computed for each of the orbits of interest, and 60 points along each orbit are selected, given varying phase angles. The unstable manifold is the eigenvector associated with the maximum eigenvalue of the STM computed between t_0 and T, with T the period of the orbit.

At each of the sampled points, a small impulse of magnitude $\varepsilon = 10^{-4}$ is applied in the direction of the unstable manifold. The resulting trajectory is then propagated until the manifold reaches a distance from the CoM of the system slightly beyond that of L_2, having $x_{sc} > 1.1\, x_{L_2}$.

This value is arbitrarily chosen: to close the zero velocity curves and to dispose of the spacecraft in a heliocentric orbit, it is necessary to be in a condition such that $x_{sc} > x_{L_2}$. The time for which the satellite travels along the unstable manifold even after this condition is met, without performing any manoeuvres, depends on the mission requirements. The further the distance from L_2, the more the manoeuvre that closes the velocity curves requires a low ΔV. At the same time, delaying disposal for months can be operationally inconvenient, especially considering that the chaotic dynamics of cislunar space can pull the spacecraft away from its expected trajectory.

In future works, how this threshold can be set in the most advantageous way possible will be analysed.

Once reached a condition such that $x_{sc} > 1.1\, x_{L_2}$, $JC_{\text{traj}} > JC_{L_2}$ is enforced, where JC_{traj} is the JC of the trajectory and JC_{L_2} is the one of L_2, equal to 3.1842.

This ensures that the JC of the trajectory exceeds that of L_2, which is equivalent to closing the velocity curves. Theoretically, this guarantees that the satellite remains outside the cislunar space permanently, having an energy that does not allow it to come back.

To enforce this, an impulse is given to the spacecraft in the velocity direction. The magnitude of the impulse is computed as:

$$\Delta V = -v \pm \sqrt{v^2 - \Delta J} \tag{21}$$

where v is the velocity of the spacecraft right before applying the manoeuvre and ΔJ is computed as:

$$\Delta J = JC_{L_2} - JC_{\text{traj}} \tag{22}$$

In Table 1 it is possible to find the results obtained for some orbits belonging to the family in EM-L_2.

For each orbit, both the minimum and maximum ΔV required to perform the manoeuvre are reported. These values correspond to different values of phase angles, respectively. With them, the time spent by the spacecraft on the manifold before executing the zero-velocity curve closure manoeuvre is also listed.

It is important to note that these are times of flight, which, in many cases, are high when considering that the EM system is being analysed. For this reason, it is necessary to proceed with a more accurate analysis in future works. For each case, the phase angles at which the manoeuvres requiring the minimum and maximum $\Delta V s$ are performed are also given, $\vartheta_{\Delta V_{\text{min}}}$ and $\vartheta_{\Delta V_{\text{max}}}$.

As expected, the minimum ΔV required to perform the manoeuvres increases with the stability of the orbits and their distance from L_2. As orbits become more stable, the difference between JC_{L_2} and JC_{traj} increases, raising the ΔV needed to perform the closing of the zero velocity curves. On the other hand, the maximum local Lyapunov exponent does not seem to have a relationship with the cost of the manoeuvre. This occurs because this index primarily measures local orbit chaoticity, which is probably less relevant than stability in this context. Indeed, the effectiveness of heliocentric disposal is more

JC [-]	3.1503	3.1108	3.0757	3.0349	3.0462	3.0627
SI [-]	473.5478	210.0326	81.6949	10.7896	1.6251	1.2062
r_p **[km]**	4.88×10^4	4.29×10^4	3.68×10^4	2.53×10^4	5.74×10^3	2.68×10^3
ΔV_{min} **[m/s]**	7.3743	13.5511	22.1778	34.9913	28.6036	29.1014
ToF man$_{\Delta V_{\text{min}}}$ **[days]**	50.7599	52.2693	80.3683	74.4939	74.7958	111.9307
$\vartheta_{\Delta V_{\text{min}}}[^\circ]$	207.4576	18.3051	353.8983	329.4915	85.4237	317.2881
$L_{\lambda\ \Delta V_{\text{min}}}$ **[-]**	4.8809	2.6613	2.3428	2.0877	4.7469	2.4062
ΔV_{max} **[m/s]**	61.0123	128.0910	201.0875	246.4497	226.4804	202.0889
ToF man$_{\Delta V_{\text{max}}}$ **[days]**	15.7534	17.8408	66.1490	34.0773	55.8995	83.2102
$\vartheta_{\Delta V_{\text{max}}}[^\circ]$	353.8983	323.3898	195.2542	219.6610	152.5424	286.7797
$L_{\lambda\ \Delta V_{\text{max}}}$ **[-]**	2.9826	2.6419	6.7797	4.7722	13.8454	2.6417
P_{inside} **[-]**	0%	0%	26.67%	0%	0%	0%
$P_{Moon\,impact}$ **[-]**	0%	0%	8.33%	0%	0%	0%
$P_{Earth\,impact}$ **[-]**	0%	0%	0%	0%	0%	0%

Table 1. Heliocentric disposal applied to some orbits of the Halo family in EM-L_2.

dependent on how quickly the trajectory reaches L_2 and departs from a stable or quasi-stable condition, which is not necessarily facilitated by high chaoticity. Therefore, no clear relationship is observed between ΔV and chaoticity in these conditions.

The parameter P_{inside} defines the percentage of trajectories remaining confined within the cislunar region, not reaching L_2 during the simulation. $P_{Moon\,impact}$ and $P_{Earth\,impact}$ are instead related to the percentage of trajectories for which an uncontrolled impact with the Moon or the Earth occurs.

Propagation is carried out for a maximum of six months, after which the trajectory is not considered an option for heliocentric disposal. For all orbits examined, disposal within this time frame is achievable for all trajectories generated, except in the case of the orbit with $JC = 3.0757$. For this orbit, the unstable manifold does not always point towards L_2. For some phase angles, it is directed towards L_1. This is why in this case, for some of the generated trajectories, effective disposal is not possible in less than six months. Interestingly, this is also the only case where a percentage of trajectories impact the Moon, while the percentage of impact with the Earth is zero for all the orbits analysed.

6. Conclusions and future works

In this study, the stability of orbits in cislunar space is addressed using the CR3BP as a fundamental model. Exploiting the system's symmetry properties and numerical continuation, families of periodic orbits of significant interest for future missions can be defined. Cislunar space is inherently chaotic, making it challenging to control orbiting objects and predict their final state based on initial conditions. Given this complexity, it is important to develop strategies to accurately design the EoL phase of a mission, leveraging the system's chaotic and unstable dynamics to achieve low-cost disposal solutions.

Various tools are employed to assess the stability of the system, including the stability index, Poincaré maps, and the maximum local Lyapunov exponent. These tools provide an initial characterisation of the stability of trajectories in cislunar space. A case study is presented where heliocentric disposal is designed for some orbits within the Halo family around EM L_2. The analysis is preliminary, but it reveals a relation between disposal cost and orbital stability.

As future work, Poincaré maps will be further analysed to identify potential graveyard orbits within the cislunar region and to study transfers between orbits with similar JCs. A key limitation of this approach is the need to carefully evaluate the chosen graveyard orbits to ensure that satellites placed on them for disposal do not pose a risk to other missions.

Additionally, it would be worthwhile to investigate whether the peaks observed in Figure 6, corresponding to highly chaotic states, could serve as initial conditions for low-cost disposal solutions. Moreover, the value of L_λ shown in the graphs is relative to a time t^* equal to one day. It would be interesting to evaluate how this parameter affects the evolution of the value of L_λ, and consequently the relationship between this index and disposal.

As described, an analysis of the relationship between the cost of heliocentric disposal and the time spent on the manifold before the zero velocity curves closure manoeuvre will also be carried out. The ultimate goal would be to analyse the different parameters characterising the system, in such a way that the optimal disposal strategy for an orbit can be determined based solely on its initial conditions. Also, it would be interesting to design a disposal trajectory that exits not only EM L_2, but also Sun-Earth L_2, defining an EoL strategy that includes a link between two different dynamical models.

7. Acknowledgements

This research has received funding as part of the work developed for the agreement n. 2023-37-HH.0 for the project "Attività tecnico-scientifiche di supporto a C-SSA/ISOC e simulazione di architetture di sensori per SST", established between ASI, Italian Space Agency, and POLIMI, Politecnico di Milano.

References

[1] Holzinger, M. J., Chow, C. C., and Garretson, P., "A primer on cislunar space," Tech. rep., Air Force Research Laboratory Greene County, OH, USA, 2021.

[2] "Artemis mission - NASA," https://www.nasa.gov/humans-in-space/artemis/. Last accessed: 16 September 2024.

[3] "Gateway - NASA," https://www.nasa.gov/mission/gateway/. Last accessed: 16 September 2024.

[4] "ESA'S annual space environment report," Tech. rep., 2024, https://www.sdo.esoc.esa.int/environment_report/Space_Environment_Report_latest.pdf.

[5] Guardabasso, P., Skoulidou, D. K., Bucci, L., Letizia, F., Lemmens, S., and Lizy-Destrez, S., "Cislunar debris mitigation: Development of a methodology to assess the sustainability of lunar missions," *72nd International Astronautical Congress (IAC), Dubai*, 2021.

[6] Armellin, R., Rasotto, M., Di Lizia, P., and Renk, F., "End-of-life disposal of libration point orbit missions: The case of Gaia," *Advances in Space Research*, Vol. 56, No. 3, 2015, pp. 461–478, doi: 10.1016/j.asr.2015.03.014.

[7] Olikara, Z. P., Gómez, G., and Masdemont, J. J., "Dynamic mechanisms for spacecraft disposal from Sun-Earth libration points," *Journal of Guidance, Control, and Dynamics*, Vol. 38, No. 10, 2015, pp. 1976–1989, doi: 10.2514/1.G000581.

[8] Colombo, C., Alessi, E. M., Van der Weg, W., Soldini, S., Letizia, F., Vetrisano, M., Vasile, M., Rossi, A., and Landgraf, M., "End-of-life disposal concepts for Libration Point Orbit and Highly Elliptical Orbit missions," *Acta Astronautica*, Vol. 110, 2015, pp. 298–312, doi: 10.1016/j.actaastro.2014.11.002.

[9] Van der Weg, W. J. and Vasile, M., "Sun-Earth L_1 and L_2 to Moon transfers exploiting natural dynamics," *Celestial Mechanics and Dynamical Astronomy*, Vol. 120, No. 3, 2014, pp. 287–308.

[10] Alessi, E. M., "The reentry to Earth as a valuable option at the end-of-life of Libration Point Orbit missions," *Advances in Space Research*, Vol. 55, No. 12, 2015, pp. 2914–2930.

[11] Szebehely, V., *Theory of Orbit: The restricted problem of three Bodies*, Academic Press, 1st ed., 1967.

[12] Koon, W. S., Lo, M. W., Marsden, J. E., and Ross, S. D., *Dynamical Systems, the Three-Body Problem and Space Mission Design*, Marsden Books, 2011.

[13] Parker, T. S. and Chua, L., *Practical numerical algorithms for chaotic systems*, Springer Science & Business Media, 1989, doi: 10.1007/978-1-4612-3486-9.

[14] Doedel, E. J., Paffenroth, R. C., Keller, H. B., Dichmann, D. J., Galán-Vioque, J., and Vanderbauwhede, A., "Computation of periodic solutions of conservative systems with application to the 3-body problem," *International Journal of Bifurcation and Chaos*, Vol. 13, No. 06, 2003, pp. 1353–1381, doi: 10.1142/S0218127403007291.

[15] Doedel, E. J., Romanov, V. A., Paffenroth, R. C., Keller, H. B., Dichmann, D. J., GalÁn-Vioque, J., and Vanderbauwhede, A., "Elemental periodic orbits associated with the libration points in the circular restricted 3-body problem," *International Journal of Bifurcation and Chaos*, Vol. 17, No. 08, 2007, pp. 2625–2677, doi: 10.1142/S0218127407018671.

[16] Hénon, M., "Numerical exploration of the restricted problem, V," *Astronomy and Astrophysics, vol. 1, p. 223-238 (1969).*, Vol. 1, 1969, pp. 223–238.

[17] Lyapunov, A. M., "The general problem of the stability of motion," *International Journal of Control*, Vol. 55, No. 3, 1992, pp. 531–534, doi: 10.1080/00207179208934253.

[18] Shore, S. N., "Celestial Mechanics," *Encyclopedia of Physical Science and Technology (Third Edition)*, edited by R. A. Meyers, Academic Press, New York, third edition ed., 2003, pp. 527–540, doi: 10.1016/B0-12-227410-5/00088-0.

[19] Connor Howell, K., "Three-dimensional, periodic,'halo'orbits," *Celestial mechanics*, Vol. 32, No. 1, 1984, pp. 53–71, doi: 10.1007/BF01358403.

[20] Skokos, C., "On the stability of periodic orbits of high dimensional autonomous Hamiltonian systems," *Physica D: Nonlinear Phenomena*, Vol. 159, No. 3-4, 2001, pp. 155–179, doi: 0.1016/S0167-2789(01)00347-5.

[21] Heggie, D. C., "Bifurcation at complex instability," *Celestial mechanics*, Vol. 35, No. 4, 1985, pp. 357–382, doi: 10.1007/BF01227832.

[22] Hénon, M., "Exploration numérique du problème restreint. II. Masses égales, stabilité des orbites périodiques," *Annales d'Astrophysique, Vol. 28, p. 992*, Vol. 28, 1965, pp. 992.

[23] Broucke, R. A., "Periodic Orbits in the Restricted Three Body Problem with Earth-Moon masses," Tech. rep., NASA, 1968.

[24] Soldini, S., *Design and control of solar radiation pressure assisted missions in the sun-earth restricted three-body problem*, Ph.D. thesis, University of Southampton, Faculty of Engineering and the Environment, 2016.

[25] Winter, O. C., "The stability evolution of a family of simply periodic lunar orbits," *Planetary and Space Science*, Vol. 48, No. 1, 2000, pp. 23–28, doi: 10.1016/S0032-0633(99)00082-3.

[26] Geisel, C. D., *Spacecraft orbit design in the circular restricted three-body problem using higher-dimensional Poincaré maps*, Ph.D. thesis, Purdue University, 2013.

[27] Celletti, A., *Stability and chaos in celestial mechanics*, Springer Science & Business Media, 2010.

[28] Pergola, P. and Alessi, E., "Libration point orbit characterization in the Earth-Moon system," *Monthly Notices of the Royal Astronomical Society*, Vol. 426, No. 2, 2012, pp. 1212–1222, doi: 10.1111/j.1365-2966.2012.21585.x.